

\mathcal{H}_2 -Norm Transmission Switching to Improve Synchronism of Low-Inertia Power Grids

Tong Han* David J.Hill*

* Department of Electrical and Electronic Engineering, The University of Hong Kong, Hong Kong. (e-mail: hantong, dhill@eee.hku.hk)

Abstract: This paper investigates the utilization of transmission switching to improve synchronization performance of low-inertia grids. The synchronization performance of power grids is first measured by the \mathcal{H}_2 norm of linearized power systems. Laplacian-based bounds and a close-form formulation of the \mathcal{H}_2 -norm synchronization performance metric are derived to reveal the influence of network structure on synchronization performance. Furthermore, a transmission switching approach is developed by analyzing the sensitivity of the \mathcal{H}_2 -norm metric to perturbation of network susceptance. Effectiveness of the proposed approach to improve synchronization performance is demonstrated using the SciGRID network for Germany.

Keywords: Transmission switching, power grids, synchronization, sensitivity

1. INTRODUCTION

Power grids are evolving toward 100% renewable energy to stem catastrophic climate change. Conventional synchronous generators, whose inertia and damping are essential for synchronism of power grids, will be steadily substituted by inverter-interfaced generation. This transition, however, can cause new challenges for power grid operations, one of which is reduction of synchronization performance due to the resulting low, time-varying and heterogeneous system inertia (Milano et al., 2018).

To tackle the deterioration of synchronism, much effort has been made to design control strategies of inverters and optimize parameters of inverter's control loop systematically. These efforts essentially improve synchronization performance by regulating node (i.e., inverter) dynamic properties of power grids. However, from a perspective of dynamic networks, not only node properties but also network structures can influence network's dynamic behaviors. For conventional or inverter-interfaced power grids, the key role of grid topology for synchronization and some stability issues has already been revealed (Huang et al., 2019; Ulbig et al., 2015; Song et al., 2017). Therefore, it is of great potential to leverage the flexibility in the topology to tackle the new challenge arising from the transition of power grids.

In transmission networks, transmission switching has been demonstrated to be effective for reducing dispatch cost (Fisher et al., 2008), relieving overload and voltage violation (Rolim and Machado, 1999; Shao and Vittal, 2005), enhancing the small-signal stability margin (Li et al., 2018), etc (Sadat and Sahraei-Ardakani, 2018; Hedman et al., 2011). In contrast to regulation of inverters' dynamic properties which requires support of energy storage devices, transmission switching, in the physical layer, only

* This work was supported by the Research Grants Council of the Hong Kong Special Administrative Region under the General Research Fund (GRF) through Project No. 17209419.

relies on breakers and communication networks which are generally fully equipped for modern power grids. Considering the high cost of large-scale energy storage, transmission switching can be one of techniques for bringing an economical package to solve synchronism and frequency stability problems of low-inertia power grids. It should be pointed out that transmission switching is unable to solve these problems individually and energy storage-based frequency regulation is still indispensable.

In this work, we utilize transmission switching as a mean to improve synchronization performance for low-inertia power grids. Contributions of this paper are twofold:

- We investigate the impact of network structure on synchronization performance measured by the \mathcal{H}_2 norm of linearized power systems, where Laplacian-based bounds and a close-form formulation of the \mathcal{H}_2 norm are derived.
- A transmission switching approach is developed to improve synchronization performance by analyzing sensitivity of the \mathcal{H}_2 norm to perturbation of network susceptance.

2. DYNAMIC MODELS

Consider a lossless transmission power grid denoted by an undirected graph $\mathcal{G}(\mathcal{V}, \mathcal{E})$ where \mathcal{V} is the set of vertices (buses) and \mathcal{E} is the set of edges (branches). The power grid is augmented with the internal buses of synchronous generators. \mathcal{V} consists of \mathcal{V}_L , \mathcal{V}_S and \mathcal{V}_{FM} , denoting sets of load buses and buses with neither load nor power generation, synchronous generator buses and grid-forming inverter buses, respectively. $\mathcal{V}_{SF} = \mathcal{V}_S \cup \mathcal{V}_{FM}$. \mathcal{V}_{SF} equals to \mathcal{V}_{SF} with the first bus deleted. $\mathcal{V} = \mathcal{V}_{SF} \cup \mathcal{V}_L$. \mathcal{E} can be divided into $\mathcal{E}_{SF} \subseteq \mathcal{V}_{SF} \times \mathcal{V}_L$ and $\mathcal{E}_L \subseteq \mathcal{V}_L \times \mathcal{V}_L$. The induced graph of \mathcal{G} by \mathcal{V}_L , denoted as $\tilde{\mathcal{G}}(\mathcal{V}_L, \mathcal{E}_L)$ contains branches which can be switched. Denote by V_i , θ_i and ω_i the voltage magnitude, voltage phase angle and angular frequency of bus i , respectively. Additionally, denote by $\mathbf{L}(\mathcal{G}, \mathbf{W})$ the

Laplacian matrix of weighted graph \mathcal{G} with \mathbf{W} being the diagonal weighted matrix, and $\mathbf{L}(\mathcal{G}, \mathbf{W})$ called the reduced Laplacian matrix, the principal matrix of $\mathbf{L}(\mathcal{G}, \mathbf{W})$ formed by deleting the first row and column. $\mathbf{E}_{\mathcal{G}}$ and $\mathbf{E}_{\tilde{\mathcal{G}}}$ are incidence matrices of \mathcal{G} and $\tilde{\mathcal{G}}$, respectively. $\underline{\mathbf{E}}_{\mathcal{G}}$ is formed by deleting the first row of $\mathbf{E}_{\mathcal{G}}$.

The structure preserving property is vital to dynamic models employed for the transmission switching problem. Hence following the previous work by Bergen and Hill (1981) and Song et al. (2017), we adopt the frequency-dependent load model and exert singular perturbation to buses with neither load nor power generation. Then the dynamic of load buses is given by

$$d_i \dot{\theta}_i = p_{in,i} - \sum_{j \in \mathcal{V}} V_i V_j b_{ij} \sin(\theta_i - \theta_j) \quad \forall i \in \mathcal{V}_L \quad (1)$$

where d_i and $p_{in,i}$ are the frequency coefficient and opposite of load power of bus i , respectively. Buses with zero power injection are regarding as load buses with d_i being singularly perturb as $d_i = \epsilon$ where ϵ is a sufficiently small positive number. b_{ij} is the susceptance between buses $(i, j) \in \mathcal{E}$. The voltage magnitude V_i of each bus is assumed to be constant.

Dynamics of synchronous generator and grid-forming inverter buses are given by

$$\begin{aligned} \dot{\theta}_i &= \omega_i \quad \forall i \in \mathcal{V}_{SF} \\ m_i \dot{\omega}_i &= -d_i \omega + p_{in,i} - \sum_{j \in \mathcal{V}} V_i V_j b_{ij} \sin(\theta_i - \theta_j) \quad \forall i \in \mathcal{V}_{SF} \end{aligned} \quad (2)$$

where m_i and d_i are the inertia (or virtual inertia) and damping coefficients of synchronous generators or grid-forming inverters, respectively; $p_{in,i}$ is the set point of active power generation.

To obtain the state-space model of power grids, we take the first bus in \mathcal{V}_{SF} as the angle reference, and a new vector is introduced as

$$\boldsymbol{\alpha} = \text{col}(\boldsymbol{\alpha}_{SF}, \boldsymbol{\alpha}_L) = \mathbf{T}\boldsymbol{\theta} \in \mathbb{R}^{|\mathcal{V}|} \quad (3)$$

with $\mathbf{T} = \text{row}(-\mathbf{1}_{|\mathcal{V}|}, \mathbf{I}_{|\mathcal{V}|}) \in \mathbb{R}^{|\mathcal{V}| \times |\mathcal{V}|}$ being the transformation matrix (Song et al., 2017). $\mathbf{T}_{SF} \in \mathbb{R}^{|\mathcal{V}| \times |\mathcal{V}_{SF}|}$ and $\mathbf{T}_L \in \mathbb{R}^{|\mathcal{V}| \times |\mathcal{V}_L|}$ consist of columns of \mathbf{T} corresponding to buses \mathcal{V}_{SF} and buses \mathcal{V}_L , respectively.

Now we consider a disturbance input vector $\Delta \mathbf{u}$ satisfying $\boldsymbol{\Lambda}^{\frac{1}{2}} \Delta \mathbf{u} = \underline{\mathbf{p}}_{in} - \underline{\mathbf{p}}_{in}^0$. $\Delta \mathbf{u} = \text{col}(\Delta \mathbf{u}_i), \forall i \in \mathcal{V}$ indicates the type of power disturbances, and $\boldsymbol{\Lambda} = \text{diag}(\Lambda_i), \forall i \in \mathcal{V}$ is the parametric matrix to model the location and strength of power disturbances. Additionally, denote by $\Delta \mathbf{y}$ the performance output vector of linearized power grids. With state variables being $\mathbf{x} = \text{col}(\boldsymbol{\alpha}, \boldsymbol{\omega}_{SF})$, the state-space model of linearization of power grids around the equilibrium point $\mathbf{x}^0 = \text{col}(\boldsymbol{\alpha}^0, \boldsymbol{\omega}_{SF}^0)$ is given as

$$\begin{bmatrix} \dot{\Delta \mathbf{x}} \\ \Delta \mathbf{y} \end{bmatrix} = \begin{bmatrix} \mathbf{A} & \mathbf{B} \\ \mathbf{C} & \mathbf{O} \end{bmatrix} \begin{bmatrix} \Delta \mathbf{x} \\ \Delta \mathbf{u} \end{bmatrix} \quad (4)$$

with

$$\mathbf{A} = \begin{bmatrix} -\mathbf{T}_L \mathbf{D}_L^{-1} \mathbf{T}_L^T \mathbf{L}(\mathcal{G}, \mathbf{W}_p) & \mathbf{T}_{SF} \\ -\mathbf{M}_{SF}^{-1} \mathbf{T}_{SF}^T \mathbf{L}(\mathcal{G}, \mathbf{W}_p) & -\mathbf{M}_{SF}^{-1} \mathbf{D}_{SF} \end{bmatrix} \quad (5)$$

$$\mathbf{B} = \begin{bmatrix} \mathbf{O} & \mathbf{T}_L \mathbf{D}_L^{-1} \boldsymbol{\Lambda}_L^{\frac{1}{2}} \\ \mathbf{M}_{SF}^{-1} \boldsymbol{\Lambda}_{SF}^{\frac{1}{2}} & \mathbf{O} \end{bmatrix} \quad (6)$$

where $\mathbf{D}_L = \text{diag}(d_i), \forall i \in \mathcal{V}_L$, $\mathbf{D}_{SF} = \text{diag}(d_i), \forall i \in \mathcal{V}_{SF}$, $\mathbf{M}_{SF} = \text{diag}(m_i), \forall i \in \mathcal{V}_{SF}$ and $\mathbf{W}_p = \mathbf{B}_V \frac{\partial \sin(\underline{\mathbf{E}}_{\mathcal{G}}^T \boldsymbol{\alpha}^0)}{\partial (\underline{\mathbf{E}}_{\mathcal{G}}^T \boldsymbol{\alpha}^0)}$ with $\mathbf{B}_V = \text{diag}(V_i V_j b_{ij}), \forall (i, j) \in \mathcal{E}$. Denote by $\mathbf{G}(s)$ the transfer matrix between the disturbance input $\Delta \mathbf{u}$ and the performance output $\Delta \mathbf{y}$.

3. SYNCHRONIZATION PERFORMANCE METRICS

Synchronization of power grids is generally understood as an integration of phase cohesiveness and frequency synchronization (or frequency boundedness) (Dörfler and Bullo, 2009; Zhu and Hill, 2018). While the extreme of angle difference and frequency determines whether the system remains synchronous, overall performance metrics to evaluate synchronism are preferred for optimization problems (Poolla et al., 2019, 2017). Here we define the following metric \mathcal{S} to evaluate the synchronization performance of power grids regarding a given disturbance with its time-domain response:

$$\begin{aligned} \mathcal{S}(T_f) &= \\ \xi(T_f, f) &= \int_0^{T_f} \left[\sum_{(i,j) \in \mathcal{E}} \mathbf{W}_{1,ij} (\Delta \theta_i - \Delta \theta_j)^2 + \sum_{i \in \mathcal{V}_{SF}} \mathbf{W}_{2,i} \Delta \omega_i^2 \right] dt \end{aligned} \quad (7)$$

where $[0, T_f]$ is the time horizon of interest; function $\xi(T_f, f)$ returns T_f when $T_f = +\infty$ and the integral term denoted as f is finite, and 1 otherwise; $\mathbf{W}_{1,ij}$ and $\mathbf{W}_{2,i}$ are positive weighting factors or scalars. Denote by \mathbf{W}_1 and \mathbf{W}_2 matrices $\text{diag}(\mathbf{W}_{1,ij})$ and $\text{diag}(\mathbf{W}_{2,i})$, respectively. $\mathcal{S}(T_f)$ expresses an average synchronization performance in time horizon $[0, T_f]$ except in the case where we consider a infinite time horizon but f is finite. In such case, $\mathcal{S}(T_f) = f$ should be understood as an accumulative synchronization performance in time horizon $[0, T_f]$. Furthermore, with matrix \mathbf{C} in (4) defined by

$$\mathbf{C} = \begin{bmatrix} \mathbf{W}_1^{\frac{1}{2}} \underline{\mathbf{E}}_{\mathcal{G}}^T & \mathbf{O} \\ \mathbf{O} & \mathbf{W}_2^{\frac{1}{2}} \end{bmatrix} \quad (8)$$

\mathcal{S} can be equivalently formulated as

$$\mathcal{S}(T_f) = \xi(T_f, f) \frac{1}{T_f} \int_0^{T_f} \Delta \mathbf{y}^T \Delta \mathbf{y} dt \quad (9)$$

With the assumption that \mathbf{A} is Hurwitz and $\Delta \mathbf{x}(0) = \mathbf{0}$, for unit impulse disturbance inputs and white noise disturbance inputs with the unit covariance matrix, $\mathcal{S}(T_f)$ with $T_f = +\infty$ or the expectation of $\mathcal{S}(T_f)$ with $T_f \rightarrow +\infty$ is further equivalent to the square of the \mathcal{H}_2 norm of $\mathbf{G}(s)$. Mathematically, we have

$$\mathcal{S}(+\infty) = \|\mathbf{G}\|_{\mathcal{H}_2}^2 \text{ if } \Delta \mathbf{u}_i = \delta(t), \forall i \in \mathcal{V} \quad (10)$$

$$\mathbb{E} \left[\lim_{T_f \rightarrow +\infty} \mathcal{S}(T_f) \right] = \|\mathbf{G}\|_{\mathcal{H}_2}^2 \text{ if } \mathbb{E}[\Delta \mathbf{u}_i] = 0, \forall i \in \mathcal{V} \text{ and } \mathbb{E}[\Delta \mathbf{u}(t) \Delta \mathbf{u}(t+\tau)^T] = \mathbf{I} \delta(\tau) \quad (11)$$

In (10), f is finite since $\Delta \mathbf{y}$ is bounded and $\lim_{t \rightarrow T_f} \Delta \mathbf{y}(t) = \Delta \mathbf{y}(0) = \mathbf{0}$, and thus $\xi(T_f, f) = T_f$. In (11), $\xi(T_f, f) = 1$ since f is infinite.

The \mathcal{H}_2 norm can be computed with observability Gramian \mathbf{P} as

$$\|\mathbf{G}\|_{\mathcal{H}_2}^2 = \text{Tr}(\mathbf{B}^T \mathbf{P} \mathbf{B}) \quad (12)$$

Here \mathbf{P} can be given by the following Lyapunov equation (Zhou et al., 1996)

$$\mathbf{A}^T \mathbf{P} + \mathbf{P} \mathbf{A} + \mathbf{C}^T \mathbf{C} = \mathbf{O} \quad (13)$$

Thereby $\|\mathbf{G}\|_{\mathcal{H}_2}$ can be interpreted as an integrated metric involving synchronization performance under different forms of disturbances, which will be employed for transmission switching.

4. IMPACT OF NETWORK STRUCTURE ON $\|\mathbf{G}\|_{\mathcal{H}_2}$

To develop the approach of transmission switching to improve synchronization performance, in this section, we investigate how network structure impacts the synchronization performance metric. Specifically, bounds of $\|\mathbf{G}\|_{\mathcal{H}_2}$ are established for general cases and the close form under certain assumptions.

4.1 Bounds of the synchronization performance metric

Theorem 1. (Laplacian-based bounds) Consider the system $(\mathbf{A}, \mathbf{B}, \mathbf{C})$ with \mathbf{A} , \mathbf{B} and \mathbf{C} given by (5) to (8) respectively, and \mathbf{D}_L , \mathbf{M}_{SF} and \mathbf{D}_{SF} being all positive definite, and then $\|\mathbf{G}\|_{\mathcal{H}_2}$ satisfies

$$\begin{aligned} \frac{\lambda_d}{2} [\text{Tr}(\mathbf{\Pi}) + \text{Tr}(\mathbf{M}_{SF}^{-1}\mathbf{W}_2)] &\leq \|\mathbf{G}\|_{\mathcal{H}_2}^2 \\ &\leq \frac{\bar{\lambda}_d}{2} [\text{Tr}(\mathbf{\Pi}) + \text{Tr}(\mathbf{M}_{SF}^{-1}\mathbf{W}_2)] \end{aligned} \quad (14)$$

where $\mathbf{\Pi} = \mathbf{L}(\mathcal{G}, \mathbf{W}_1)\mathbf{L}(\mathcal{G}, \mathbf{W}_p)^{-1}$, $\lambda_d = \min_{i \in \mathcal{V}} \{\frac{\Lambda_i}{d_i}\}$ and $\bar{\lambda}_d = \max_{i \in \mathcal{V}} \{\frac{\Lambda_i}{d_i}\}$.

Proof. Partitioning \mathbf{P} as

$$\mathbf{P} = \begin{bmatrix} \mathbf{P}_{11} & \mathbf{P}_{12} \\ \mathbf{P}_{12}^T & \mathbf{P}_{22} \end{bmatrix}, \quad (15)$$

we have

$$\|\mathbf{G}\|_{\mathcal{H}_2}^2 = \text{Tr}(\mathbf{\Lambda}_L \mathbf{D}_L^{-2} \mathbf{T}_L^T \mathbf{P}_{11} \mathbf{T}_L) + \text{Tr}(\mathbf{\Lambda}_{SF} \mathbf{M}_{SF}^{-2} \mathbf{P}_{22}) \quad (16)$$

The Lyapunov equation (13) can be expanded as

$$\mathbf{A}^T \begin{bmatrix} \mathbf{P}_{11} & \mathbf{P}_{12} \\ \mathbf{P}_{12}^T & \mathbf{P}_{22} \end{bmatrix} + \begin{bmatrix} \mathbf{P}_{11} & \mathbf{P}_{12} \\ \mathbf{P}_{12}^T & \mathbf{P}_{22} \end{bmatrix} \mathbf{A} + \begin{bmatrix} \mathbf{L}(\mathcal{G}, \mathbf{W}_1) & \mathbf{O} \\ \mathbf{O} & \mathbf{W}_2 \end{bmatrix} = \mathbf{O} \quad (17)$$

Assume that the graph $\tilde{\mathcal{G}}$ is connected and thus matrix $\mathbf{L}(\mathcal{G}, \mathbf{W}_p)$ is nonsingular. Note that $\mathbf{L}(\mathcal{G}, \mathbf{W}_p)$ is also symmetric. Right-multiplying equation (1,1) of (17) by $\mathbf{L}(\mathcal{G}, \mathbf{W}_p)^{-1}$ gives

$$\begin{aligned} &\mathbf{L}(\mathcal{G}, \mathbf{W}_p)^T \mathbf{T}_L \mathbf{D}_L^{-1} \mathbf{T}_L^T \mathbf{P}_{11} \mathbf{L}(\mathcal{G}, \mathbf{W}_p)^{-1} \\ &+ \mathbf{L}(\mathcal{G}, \mathbf{W}_p)^T \mathbf{T}_{SF} \mathbf{M}_{SF}^{-1} \mathbf{P}_{12}^T \mathbf{L}(\mathcal{G}, \mathbf{W}_p)^{-1} \\ &+ \mathbf{P}_{11} \mathbf{T}_L \mathbf{D}_L^{-1} \mathbf{T}_L^T \mathbf{L}(\mathcal{G}, \mathbf{W}_p) \mathbf{L}(\mathcal{G}, \mathbf{W}_p)^{-1} \\ &+ \mathbf{P}_{12} \mathbf{M}_{SF}^{-1} \mathbf{T}_{SF}^T \mathbf{L}(\mathcal{G}, \mathbf{W}_p) \mathbf{L}(\mathcal{G}, \mathbf{W}_p)^{-1} = \mathbf{\Pi} \end{aligned} \quad (18)$$

With 1) the cyclic property of trace, 2) trace invariance of transpose, and 3) the equality that $\mathbf{L}(\mathcal{G}, \mathbf{W}_p)\mathbf{L}(\mathcal{G}, \mathbf{W}_p)^{-1} = \mathbf{I}$, we obtain the following trace equality from (18)

$$\text{Tr}(\mathbf{T}_L \mathbf{D}_L^{-1} \mathbf{T}_L^T \mathbf{P}_{11}) + \text{Tr}(\mathbf{P}_{12} \mathbf{M}_{SF}^{-1} \mathbf{T}_{SF}^T) = \frac{1}{2} \text{Tr}(\mathbf{\Pi}) \quad (19)$$

Left-multiplying equation (2,2) of (17) by \mathbf{M}_{SF}^{-1} gives that

$$\text{Tr}(\mathbf{M}_{SF}^{-2} \mathbf{D}_{SF} \mathbf{P}_{22}) - \text{Tr}(\mathbf{M}_{SF}^{-1} \mathbf{T}_{SF}^T \mathbf{P}_{12}) = \frac{1}{2} \text{Tr}(\mathbf{M}_{SF}^{-1} \mathbf{W}_2) \quad (20)$$

Since the matrices in a trace of a product can be switched without changing the result, we have $\text{Tr}(\mathbf{P}_{12} \mathbf{M}_{SF}^{-1} \mathbf{T}_{SF}^T) = \text{Tr}(\mathbf{M}_{SF}^{-1} \mathbf{T}_{SF}^T \mathbf{P}_{12})$. Thus combining (19) and (20) gives that

$$\begin{aligned} &\text{Tr}(\mathbf{T}_L \mathbf{D}_L^{-1} \mathbf{T}_L^T \mathbf{P}_{11}) + \text{Tr}(\mathbf{M}_{SF}^{-2} \mathbf{D}_{SF} \mathbf{P}_{22}) \\ &= \frac{1}{2} \text{Tr}(\mathbf{\Pi}) + \frac{1}{2} \text{Tr}(\mathbf{M}_{SF}^{-1} \mathbf{W}_2) \end{aligned} \quad (21)$$

Positive semi-definiteness of \mathbf{P} , \mathbf{D}_L , \mathbf{M}_{SF} and \mathbf{D}_{SF} indicates that $\mathbf{D}_L \mathbf{T}_L^T \mathbf{P}_{11} \mathbf{T}_L$ and $\mathbf{M}_{SF}^{-2} \mathbf{D}_{SF} \mathbf{P}_{22}$ are also positive semi-definite. Therefore by Fang et al. (1994, Theorem 2), the following inequality can be established from (16):

$$\lambda_{d,L} \text{Tr}(\mathbf{D}_L^{-1} \mathbf{T}_L^T \mathbf{P}_{11} \mathbf{T}_L) + \lambda_{d,SF} \text{Tr}(\mathbf{M}_{SF}^{-2} \mathbf{D}_{SF} \mathbf{P}_{22}) \leq \|\mathbf{G}\|_{\mathcal{H}_2}^2 \quad (22)$$

where $\lambda_{d,L} = \min_{i \in \mathcal{V}_L} \{\frac{\Lambda_i}{d_i}\}$ and $\bar{\lambda}_{d,L} = \max_{i \in \mathcal{V}_L} \{\frac{\Lambda_i}{d_i}\}$, $\lambda_{d,SF} = \min_{i \in \mathcal{V}_{SF}} \{\frac{\Lambda_i}{d_i}\}$ and $\bar{\lambda}_{d,SF} = \max_{i \in \mathcal{V}_{SF}} \{\frac{\Lambda_i}{d_i}\}$,

Furthermore, by relaxing $\lambda_{d,L}$ and $\lambda_{d,SF}$ to λ_d , and $\bar{\lambda}_{d,L}$ and $\bar{\lambda}_{d,SF}$ to $\bar{\lambda}_d$, we have

$$\begin{aligned} &\lambda_d [\text{Tr}(\mathbf{D}_L^{-1} \mathbf{T}_L^T \mathbf{P}_{11} \mathbf{T}_L) + \text{Tr}(\mathbf{M}_{SF}^{-2} \mathbf{D}_{SF} \mathbf{P}_{22})] \leq \|\mathbf{G}\|_{\mathcal{H}_2}^2 \\ &\leq \bar{\lambda}_d [\text{Tr}(\mathbf{D}_L^{-1} \mathbf{T}_L^T \mathbf{P}_{11} \mathbf{T}_L) + \text{Tr}(\mathbf{M}_{SF}^{-2} \mathbf{D}_{SF} \mathbf{P}_{22})] \end{aligned} \quad (23)$$

With the equality $\text{Tr}(\mathbf{D}_L^{-2} \mathbf{T}_L^T \mathbf{P}_{11} \mathbf{T}_L) = \text{Tr}(\mathbf{T}_L \mathbf{D}_L^{-2} \mathbf{T}_L^T \mathbf{P}_{11})$, substituting (21) into (23) gives the bounds in Theorem 1. \square

Remark 1. Analogue bounds were also derived by Poolla et al. (2017) using a network-reduced dynamic model, in which, however, the influence of original network structure and load dynamics can not be observed. Note that bounds in Theorem 1 are tighter than that derived by Poolla et al. (2017). Theorem 1 reveals that $\|\mathbf{G}\|_{\mathcal{H}_2}$ can be impacted by damping and inertia of generators/inverters, damping of load, disturbance strength, and network structure embodied in $\mathbf{L}(\mathcal{G}, \mathbf{W}_1)$ and $\mathbf{L}(\mathcal{G}, \mathbf{W}_p)$. Corresponding to the first two factors, countermeasures including load-side control and allocating virtual inertia and damping have already been proved to be effective to enhance synchronism of low-inertia power grids. Transmission switching that changes network structure can promisingly achieve the same effect.

In Theorem 1, bounds of $\|\mathbf{G}\|_{\mathcal{H}_2}$ are defined in terms of reduced Laplacian matrices of graph \mathcal{G} that corresponds to the augmented power grid. To further state the bounds in terms of Laplacian matrices of graph $\tilde{\mathcal{G}}$ that correspond to the unaugmented power grid, we partition $\mathbf{L}(\mathcal{G}, \mathbf{W}_p)$ as

$$\mathbf{L}(\mathcal{G}, \mathbf{W}_p) = \begin{bmatrix} \mathbf{L}_{HH} & \mathbf{L}_{EH}^T \\ \mathbf{L}_{EH} & \mathbf{L}_{EE} \end{bmatrix} \quad (24)$$

where $\mathbf{L}_{HH} = \mathbf{T}_{SF}^T \mathbf{L}(\mathcal{G}_1, \mathbf{W}_{p1}) \mathbf{T}_{SH}$, $\mathbf{L}_{EH} = \mathbf{T}_L^T \mathbf{L}(\mathcal{G}_1, \mathbf{W}_{p1}) \mathbf{T}_{SF}$, and $\mathbf{L}_{EE} = \mathbf{L}(\tilde{\mathcal{G}}, \tilde{\mathbf{W}}_p) + \mathbf{T}_L^T \mathbf{L}(\mathcal{G}_1, \mathbf{W}_{p1}) \mathbf{T}_L$; $\mathcal{G}_1 = \mathcal{G}_1(\mathcal{V}, \mathcal{E}_{SF})$; $\mathbf{W}_{p1} = \mathbf{B}_{V,1} \frac{\partial \sin(\mathbf{E}_{G_1}^T \boldsymbol{\alpha}^0)}{\partial (\mathbf{E}_{G_1}^T \boldsymbol{\alpha}^0)}$ with \mathbf{E}_{G_1} formed by deleting the first row of the incidence matrix of \mathcal{G}_1 and $\mathbf{B}_{V,1} = \text{diag}(V_i V_j b_{ij}), \forall (i, j) \in \mathcal{E}_{SF}$.

Correspondingly, $\mathbf{L}(\mathcal{G}, \mathbf{W}_1)$ can be formulated as the following block form

$$\mathbf{L}(\mathcal{G}, \mathbf{W}_1) = \begin{bmatrix} \mathbf{L}_{HH}^* & \mathbf{L}_{EH}^{*T} \\ \mathbf{L}_{EH}^* & \mathbf{L}_{EE}^* \end{bmatrix}. \quad (25)$$

Lemma 2. The following equality holds

$$\text{Tr}(\mathbf{\Pi}) = \text{Tr}(\mathbf{L}_S^* \mathbf{L}_S^{-1}) + \text{Tr}(\mathbf{L}_{HH}^* \mathbf{L}_{HH}^{-1}) \quad (26)$$

where $\mathbf{L}_S^* = \mathbf{L}(\tilde{\mathcal{G}}, \tilde{\mathbf{W}}_1) + \boldsymbol{\Theta}^*$ and $\mathbf{L}_S = \mathbf{L}(\tilde{\mathcal{G}}, \tilde{\mathbf{W}}_p) + \boldsymbol{\Theta}$; $\tilde{\mathbf{W}}_1$ is the principal sub-matrix of \mathbf{W}_1 indexed by \mathcal{E}_L ;

$\widetilde{\mathbf{W}}_p = \widetilde{\mathbf{B}}_V \frac{\partial \sin(\mathbf{E}_G^T \boldsymbol{\alpha}_L^0)}{\partial (\mathbf{E}_G^T \boldsymbol{\alpha}_L^0)}$ with $\widetilde{\mathbf{B}}_V = \text{diag}(V_i V_j b_{ij}), \forall (i, j) \in \mathcal{E}_L$;
 $\boldsymbol{\Theta}^* = \text{diag}(\mathbf{W}_{1,ij}, 0, \dots, 0) \in \mathbb{R}^{|\mathcal{V}_L| \times |\mathcal{V}_L|}$ with bus i being the angle reference bus and j being its adjacent bus;
 $\boldsymbol{\Theta} = \text{diag}(\mathbf{W}_{p1}^{(1)}, 0, \dots, 0) \in \mathbb{R}^{|\mathcal{V}_L| \times |\mathcal{V}_L|}$ with $\mathbf{W}_{p1}^{(1)}$ being the first element of \mathbf{W}_{p1} .

Proof. Under the assumption that $\|\text{diag}(\mathbf{W}_{p1})\|_{-\infty} > 0$, \mathbf{L}_{HH} is diagonal and also non-singular. Then the Schur complement of \mathbf{L}_{HH} is given by

$$\begin{aligned} \mathbf{L}_S &= \mathbf{L}_{EE} - \mathbf{L}_{EH} \mathbf{L}_{HH}^{-1} \mathbf{L}_{HE} \\ &= \mathbf{L}(\widetilde{\mathcal{G}}, \widetilde{\mathbf{W}}_p) + \mathbf{T}_L^T \underline{\mathbf{L}}(\mathcal{G}_1, \mathbf{W}_{p1}) \mathbf{T}_L - \mathbf{L}_{EH} \mathbf{L}_{HH}^{-1} \mathbf{L}_{HE} \\ &= \mathbf{L}(\widetilde{\mathcal{G}}, \widetilde{\mathbf{W}}_p) + \mathbf{T}_L^T \underline{\mathbf{L}}(\mathcal{G}_1, \mathbf{W}_{p1}) \mathbf{T}_L - \mathbf{E}_I \mathbf{T}_{SF}^T \underline{\mathbf{L}}(\mathcal{G}_1, \mathbf{W}_{p1}) \mathbf{T}_L \\ &= \mathbf{L}(\widetilde{\mathcal{G}}, \widetilde{\mathbf{W}}_p) + \boldsymbol{\Theta} \end{aligned} \quad (27)$$

where $\mathbf{E}_I = \mathbf{T}_L^T \underline{\mathbf{E}}_G \mathbf{E}_G^T \mathbf{T}_{SF}$.

Furthermore, by Meyer (2000, Problem 3.7.11) and equalities that $\mathbf{L}_{EH} \mathbf{L}_{HH}^{-1} = \mathbf{E}_I$ and $\mathbf{L}_{HH}^{-1} \mathbf{L}_{EH}^T = \mathbf{E}_I^T$, we have

$$\underline{\mathbf{L}}(\mathcal{G}, \mathbf{W}_p)^{-1} = \begin{bmatrix} \mathbf{L}_{HH}^{-1} + \mathbf{E}_I^T \mathbf{L}_S^{-1} \mathbf{E}_I & -\mathbf{E}_I^T \mathbf{L}_S^{-1} \\ -\mathbf{L}_S^{-1} \mathbf{E}_I & \mathbf{L}_S^{-1} \end{bmatrix} \quad (28)$$

Substituting (28) and (25) into $\boldsymbol{\Pi}$ yields

$$\begin{aligned} \text{Tr}(\boldsymbol{\Pi}) &= \text{Tr}((\mathbf{L}_{EE}^* - \mathbf{L}_{EH}^* \mathbf{E}_I^T) \mathbf{L}_S^{-1}) + \text{Tr}(\mathbf{L}_{HH}^* \mathbf{L}_{HH}^{-1}) \\ &\quad + \text{Tr}((\mathbf{L}_{HH}^* \mathbf{E}_I^T - \mathbf{L}_{HE}^*) \mathbf{L}_S^{-1} \mathbf{E}_I) \end{aligned} \quad (29)$$

which together with $\mathbf{L}_S^* = \mathbf{L}_{EE}^* - \mathbf{L}_{EH}^* \mathbf{E}_I^T$ and $\mathbf{L}_{HH}^* \mathbf{E}_I^T = \mathbf{L}_{HE}^*$ gives Lemma 2. \square

Remark 2. Matrix \mathbf{L}_S can be interpreted as the Laplacian matrix of graph $\widetilde{\mathcal{G}}$ added one self-loop at the load node connected with the angle reference bus. The weight of the self-loop equals to the nonzero elements in $\boldsymbol{\Theta}$ which is positive. Matrix \mathbf{L}_S^* is analogue.

By Lemma 2, bounds in Theorem 1 is restate in terms of Laplacian matrices of $\widetilde{\mathcal{G}}$ as follows:

Corollary 3. Consider the system $(\mathbf{A}, \mathbf{B}, \mathbf{C})$ with \mathbf{A} , \mathbf{B} and \mathbf{C} given by (5) to (8) respectively, and \mathbf{D}_L , $\underline{\mathbf{M}}_{SF}$ and $\underline{\mathbf{D}}_{SF}$ being all positive definite, and then $\|\mathbf{G}\|_{\mathcal{H}_2}$ satisfies

$$\begin{aligned} &\frac{\lambda_d}{2} [\text{Tr}(\mathbf{L}_S^* \mathbf{L}_S^{-1}) + \text{Tr}(\mathbf{L}_{HH}^* \mathbf{L}_{HH}^{-1} + \underline{\mathbf{M}}_{SF}^{-1} \mathbf{W}_2)] \leq \|\mathbf{G}\|_{\mathcal{H}_2}^2 \\ &\leq \frac{\bar{\lambda}_d}{2} [\text{Tr}(\mathbf{L}_S^* \mathbf{L}_S^{-1}) + \text{Tr}(\mathbf{L}_{HH}^* \mathbf{L}_{HH}^{-1} + \underline{\mathbf{M}}_{SF}^{-1} \mathbf{W}_2)] \end{aligned} \quad (30)$$

Remark 3. In each bound in Corollary 3, only the first trace term is dependent on structure of the unaugmented power grids. \mathbf{L}_S^* and \mathbf{L}_S are Laplacian matrices of $\widetilde{\mathcal{G}}$ add one self-loop, whose edge weights are related to weighting factors in \mathcal{S} and active power flow at the equilibrium point, respectively.

Furthermore, under Assumption 1, the synchronization performance metric $\|\mathbf{G}\|_{\mathcal{H}_2}$ can be formulated in close form, for which the observability Gramian is eliminated.

Assumption 1. The ratio of disturbance strength to load damping and that of disturbance strength to generator/inverter damping are uniform, i.e., $\frac{\lambda_i}{d_i} = \lambda_d, \forall i \in \mathcal{V}_L \cup \underline{\mathcal{V}}_{SF}$.

Corollary 4. ($\|\mathbf{G}\|_{\mathcal{H}_2}$ under Assumption 1) Consider the system $(\mathbf{A}, \mathbf{B}, \mathbf{C})$ with \mathbf{A} , \mathbf{B} and \mathbf{C} given by (5) to (8) respectively, Assumption 1 satisfied, and \mathbf{D}_L , $\underline{\mathbf{M}}_{SF}$ and $\underline{\mathbf{D}}_{SF}$ being all positive definite. Then

$$\|\mathbf{G}\|_{\mathcal{H}_2}^2 = \frac{\lambda_d}{2} [\text{Tr}(\mathbf{L}_S^* \mathbf{L}_S^{-1}) + \text{Tr}(\mathbf{L}_{HH}^* \mathbf{L}_{HH}^{-1} + \underline{\mathbf{M}}_{SF}^{-1} \mathbf{W}_2)] \quad (31)$$

Proof. Assumption 1 indicates that $\lambda_d = \bar{\lambda}_d = \lambda_d$. Then by Corollary 3, we conclude Corollary 4. \square

Remark 4. For practical power grids, Assumption 1 is reasonable since that strength of disturbances is approximately proportional to the load power or generation power while the same for the damping of loads and generators/inverters. Or to be exact, Theorem 1 and Corollary 4 provide tight bounds of $\|\mathbf{G}\|_{\mathcal{H}_2}$ for practical power grids since $\lambda_d \approx \bar{\lambda}_d$.

5. SENSITIVITY-BASED TRANSMISSION SWITCHING APPROACH

The transmission switching problem is traditionally tackled by optimization-based approaches where some steady-state metrics are generally concerned. However, finding the optimal network topology that minimizes $\|\mathbf{G}\|_{\mathcal{H}_2}$ is far from easy whether based on the Lyapunov equation or the close-form $\|\mathbf{G}\|_{\mathcal{H}_2}$. In this section, we develop a transmission switching approach by analyzing the sensitivity of $\|\mathbf{G}\|_{\mathcal{H}_2}^2$ or its bounds to perturbation of network susceptance.

5.1 Sensitivity Analysis

Since the sensitivity of close-form $\|\mathbf{G}\|_{\mathcal{H}_2}^2$ is proportional to that of its bounds, we only focus on the former. Sensitivity of $\|\mathbf{G}\|_{\mathcal{H}_2}^2$ to perturbation of branch susceptance is given by the following proposition.

Proposition 5. ($\partial \|\mathbf{G}\|_{\mathcal{H}_2}^2 / \partial b_{ij}$ under Assumption 1) Consider the system $(\mathbf{A}, \mathbf{B}, \mathbf{C})$ with \mathbf{A} , \mathbf{B} and \mathbf{C} given by (5) to (8) respectively, Assumption 1 satisfied, and \mathbf{D}_L , $\underline{\mathbf{M}}_{SF}$ and $\underline{\mathbf{D}}_{SF}$ being all positive definite. Then $\forall (i, j) \in \mathcal{E}_L$, we have

$$\frac{\partial \|\mathbf{G}\|_{\mathcal{H}_2}^2}{\partial b_{ij}} = -\frac{\lambda_d}{2} \text{Tr}(\mathbf{L}_S^{-1} \mathbf{L}_S^* \mathbf{L}_S^{-1} \mathbf{L}(\widetilde{\mathcal{G}}, \widetilde{\mathbf{W}}_p \mathbf{E}^{ij})) < 0 \quad (32)$$

where $\mathbf{E}^{ij} \in \mathbb{R}^{|\mathcal{E}_L| \times |\mathcal{E}_L|}$ is a diagonal matrix with only one non-zero element being $\frac{1}{b_{ij}}$ for edge (i, j) .

Proof. In the right-hand side of (31), network susceptance only appears in \mathbf{L}_S . Thus

$$\frac{\partial \|\mathbf{G}\|_{\mathcal{H}_2}^2}{\partial b_{ij}} = \frac{\lambda_d}{2} \frac{\partial \text{Tr}(\mathbf{L}_S^* \mathbf{L}_S^{-1})}{\partial b_{ij}} = \frac{\lambda_d}{2} \text{Tr}(\mathbf{L}_S^* \frac{\partial \mathbf{L}_S^{-1}}{\partial b_{ij}}) \quad (33)$$

with

$$\frac{\partial \mathbf{L}_S^{-1}}{\partial b_{ij}} = -\mathbf{L}_S^{-1} \frac{\partial \mathbf{L}_S}{\partial b_{ij}} \mathbf{L}_S^{-1} = -\mathbf{L}_S^{-1} \mathbf{L}(\widetilde{\mathcal{G}}, \widetilde{\mathbf{W}}_p \mathbf{E}^{ij}) \mathbf{L}_S^{-1}, \quad (34)$$

which together with the cyclic property of trace gives the equality in (32).

Furthermore, by Acikmese (2015, Lemma 1), $\mathbf{L}_S \succ 0$, $\mathbf{L}_S^* \succ 0$ and thus $\mathbf{L}_S^{-1} \succ 0$. Therefore, $\mathbf{L}_S^{-1} \mathbf{L}_S^* \mathbf{L}_S^{-1} \succ 0$ and its smallest eigenvalue $\lambda_{\min} > 0$. $\mathbf{L}(\widetilde{\mathcal{G}}, \widetilde{\mathbf{W}}_p \mathbf{E}^{ij})$ is with eigenvalues $\lambda_0 = \lambda_1 = \dots = \lambda_{|\mathcal{V}_L|-1} = 0 < \lambda_{|\mathcal{V}_L|}$, which gives that $\text{Tr}(\mathbf{L}(\widetilde{\mathcal{G}}, \widetilde{\mathbf{W}}_p \mathbf{E}^{ij})) > 0$. Then by Fang et al. (1994, Theorem 2), the following inequality holds:

$$\text{Tr}(\mathbf{L}_S^{-1} \mathbf{L}_S^* \mathbf{L}_S^{-1} \mathbf{L}(\widetilde{\mathcal{G}}, \widetilde{\mathbf{W}}_p \mathbf{E}^{ij})) \geq \lambda_{\min} \text{Tr}(\mathbf{L}(\widetilde{\mathcal{G}}, \widetilde{\mathbf{W}}_p \mathbf{E}^{ij})) > 0 \quad (35)$$

which together with $\lambda_d > 0$ concludes the inequality in (32). \square

Remark 5. Proposition 5 indicates that under Assumption 1, a positive perturbation of branch susceptance always decreases $\|\mathbf{G}\|_{\mathcal{H}_2}$.

5.2 Transmission Switching Approach

The transmission switching problem considered to solve is described as follows:

Problem 1. Given \mathbf{p}_{in}^0 , a initial network topology $\tilde{\mathcal{G}}(\mathcal{V}, \mathcal{E}_{L,u})$ where $\mathcal{E}_{L,u}$ is the set of undispachable branches, and a dispachable line set $\mathcal{E}_{L,s}$, find a line set $\mathcal{E}_{L,on} \subset \mathcal{E}_{L,s}$ satisfying $|\mathcal{E}_{L,on}| = n_{\text{on}}$ with n_{on} being the maximum number of lines to switch on, such that $\tilde{\mathcal{G}}(\mathcal{V}, \mathcal{E}_{L,u} \cup \mathcal{E}_{L,on})$ minimizes $\|\mathbf{G}\|_{\mathcal{H}_2}$.

In theory, Problem 1 is NP-hard while for practical implementation, it is preferred to obtain a good solution within the time available. Based on the sensitivity analysis, we can easily determine the next best line to switch on, which cannot guarantee optimality but may provide good solutions fast. Thereby we can develop an approach to solve Problem 1 by switching on one line at a time, which is given by Algorithm 1. A total of n_{on} iterations are required, in each of which we mainly need to compute power flow and inverse of \mathbf{L}_S both once.

Algorithm 1 Transmission switching approach.

Input: $\mathbf{p}_{\text{in}}^0, \tilde{\mathcal{G}}(\mathcal{V}, \mathcal{E}_{L,u}), \mathcal{E}_{L,s}, n_{\text{on}}$

Output: $\mathcal{E}_{L,on}$

- 1: Initialize $\mathcal{E}_{L,on} \leftarrow \emptyset$;
 - 2: **repeat**
 - 3: $\tilde{\mathbf{W}}_p \leftarrow$ Compute power flow for $\tilde{\mathcal{G}}(\mathcal{V}_L, \mathcal{E}_{L,u} \cup \mathcal{E}_{L,s})$
 with $\forall(i, j) \in \mathcal{E}_{L,s} - \mathcal{E}_{L,on}, b_{ij} = 0$ and $\forall(i, j) \in \mathcal{E}_{L,on}, b_{ij}$ being its actual value;
 - 4: Compute \mathbf{L}_S^{-1} and \mathbf{L}_S^* ;
 - 5: $\forall(i, j) \in \mathcal{E}_{L,s} - \mathcal{E}_{L,on}$, compute $\partial \|\mathbf{G}\|_{\mathcal{H}_2}^2 / \partial b_{ij}$;
 - 6: $\mathcal{E}_{L,on} \leftarrow \mathcal{E}_{L,on} + \arg \max_{(i,j) \in \mathcal{E}_{L,s} - \mathcal{E}_{L,on}} \partial \|\mathbf{G}\|_{\mathcal{H}_2}^2 / \partial b_{ij}$;
 - 7: **until** $|\mathcal{E}_{L,on}| = n_{\text{on}}$
 - 8: **return** $\mathcal{E}_{L,on}$
-

6. NUMERICAL EXAMPLES

In the following, the transmission switching approach to improve synchronization of power grids is tested using the SciGRID network for Germany with its load snapshot at 12:00:00 January 1st, 2011 (Han, 2019) and dispatch of generators being optimized by the linear OPF. Fig. 1 shows the main topology of the grid. This grid contains 585 buses including 489 generator/inverter buses and 485 load buses, 852 lines (multi-circuits lines are transformed into one-circuit lines) and 96 transformers. To carry out transmission switching, it is assumed that 60 lines (colored by purple and blue in Fig. 1) are dispatchable and $n_{\text{on}} = 20$.

6.1 Switching results

Fig. 2 (left) shows sensitivity values of dispatchable lines during iteration, and the line marked by a grey dot is with the largest sensitivity within the current iteration and selected to switch on. All lines to switch on, i.e., $\mathcal{E}_{L,on}$, is also colored by blue in Fig. 1. It is found that sensitivity values of some lines (e.g., line 1 and line 59) vary widely

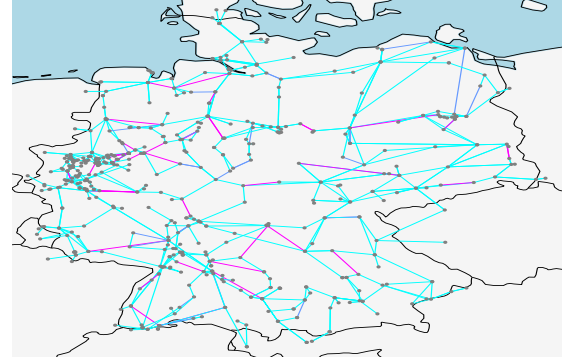


Fig. 1. Topology of the SciGRID network for Germany.

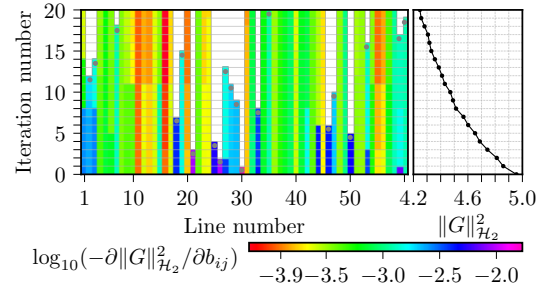


Fig. 2. Sensitivity values in each iteration (left) and change of $\|\mathbf{G}\|_{\mathcal{H}_2}^2$ with lines switched on in turn (right). Lines to switch on are marked by grey dots in the left figure.

during iteration, which indicates that switching of one line can influence the potential of remaining dispatchable lines to improve synchronization performance. This influence prevents us increasing the number of lines selected to switch on in each iteration, which though can accelerate computation.

Fig. 2 (right) is the change curve of $\|\mathbf{G}\|_{\mathcal{H}_2}^2$ with lines selected in each iteration switched on in turn. With more lines switched on, synchronization performance is continually improved while overall, the absolute value of slope of the curve decreases. These two trends correspond with negativness of $\partial \|\mathbf{G}\|_{\mathcal{H}_2}^2 / \partial b_{ij}$ and a observation from Fig. 2 (left) that $\partial \|\mathbf{G}\|_{\mathcal{H}_2}^2 / \partial b_{ij}$ decreases overall as the iteration number increases, respectively.

6.2 Output Response to time-varying disturbances

We further compare output response of the power grid with and without lines in $\mathcal{E}_{L,on}$ switched on. As mentioned in Section 3, $\|\mathbf{G}\|_{\mathcal{H}_2}^2$ implies synchronization performance in terms of white noise disturbance inputs which in fact, never disturb physical power grids. Thus taking into account the actual situation, $\forall i \in \mathcal{V}$, we set $\Delta \mathbf{u}_i$ as a time-varying signal which changes its value randomly at a equal interval 2 s according to a truncated normal distribution with mean 0, variance 1 and interval $[-1, 1]$.

Fig. 3 and Fig. 4 show the output response to the time-varying disturbances with and without line switching. In the scatter plots, $E(|\Delta \theta_{ij}|)$ (or $E(|\Delta f_i|)$) is the mean of $\Delta \theta_{ij}$ (or $E(|\Delta f_i|)$) obtained by sampling the output response, and a dot under the dashed line indicates that corresponding $E(|\Delta \theta_{ij}|)$ (or $E(|\Delta f_i|)$) is reduced after switching on lines in $\mathcal{E}_{L,on}$. In Fig. 3 (left), a dis-

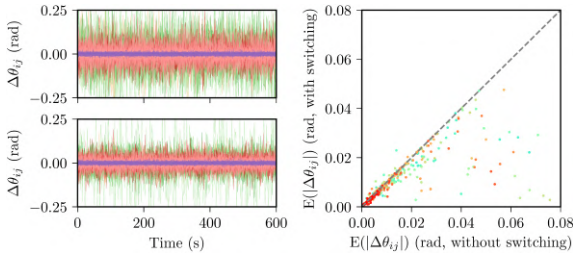


Fig. 3. Output response $\Delta\theta_{ij} = \Delta\theta_i - \Delta\theta_j$ to time-varying disturbances with (left top) and without (left bottom) line switching, and scatter plot of $E(|\Delta\theta_{ij}|)$ (right).

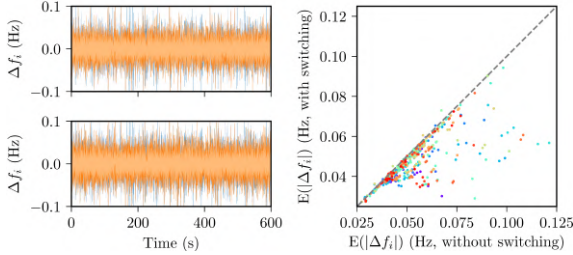


Fig. 4. Output response $\Delta f_i = \frac{\Delta\omega}{2\pi}$ to time-varying disturbances with (left top) and without (left bottom) line switching, and scatter plot of $E(|\Delta f_i|)$ (right).

tinct shrink of the curve cluster, connoting improvement of phase cohesiveness, can be observed after lines being switched on. Fig. 4 (left) provides no obvious indication of change of frequency synchronization performance. Fig. 3 (right) and Fig. 4 (right) both show that most dots are below the dashed line and therefore, phase cohesiveness of most branches and frequency synchronization performance of most generators/inverters are both improved by line switching. Phase cohesiveness of several branches is slightly undermined after lines being switched on and in general, branches with the worst pre-switch phase cohesiveness present the greatest performance improvement. Frequency synchronization performance is analogous.

7. CONCLUSION

In response to new challenges caused by transition of power grids, structure-oriented control and optimization should play a more important role than ever before. In this paper, we propose to utilize transmission switching as a mean to improve synchronization performance of grids and develop a sensitivity-based switching approach. However, it should be pointed out that the transmission switching approach developed in this paper is still far from practical application. Impact of switching on other aspects of system performance, such as transient stability and line overload, should be considered while determining lines to switch. Switching approaches that are able to tackle more general switching scenarios are expected. Coordination of transmission switching and regulation of node dynamic properties could be the final package to pursue.

REFERENCES

Acikmese, B. (2015). Spectrum of laplacians for graphs with self-loops. *arXiv preprint arXiv:1505.08133*.
 Bergen, A.R. and Hill, D.J. (1981). A structure preserving model for power system stability analysis. *IEEE Trans-*

actions on Power Apparatus and Systems, PAS-100(1), 25–35. doi:10.1109/TPAS.1981.316883.
 Dörfler, F. and Bullo, F. (2009). Synchronization and transient stability in power networks and non-uniform kuramoto oscillators. *50(3)*, 930–937.
 Fang, Y., Loparo, K.A., and Feng, X. (1994). Inequalities for the trace of matrix product. *IEEE Transactions on Automatic Control*, 39(12), 2489–2490.
 Fisher, E.B., Oneill, R.P., and Ferris, M.C. (2008). Optimal transmission switching. *IEEE Transactions on Power Systems*, 23(3), 1346–1355.
 Han, T. (2019). The scigrid network for germany. URL <https://github.com/thanever/SOC/tree/master/Data/scigrid-de>.
 Hedman, K.W., Oren, S.S., and O’Neill, R.P. (2011). A review of transmission switching and network topology optimization. In *Power and Energy Society General Meeting, 2011 IEEE*, 1–7. IEEE.
 Huang, L., Xin, H., Dong, W., and Dorfler, F. (2019). Impacts of grid structure on pll-synchronization stability of converter-integrated power systems. *arXiv preprint arXiv:1903.05489*.
 Li, C., Chiang, H.D., and Du, Z. (2018). Online line switching method for enhancing the small-signal stability margin of power systems. *IEEE Transactions on Smart Grid*, 9(5), 4426–4435.
 Meyer, C.D. (2000). *Matrix analysis and applied linear algebra*, volume 71. Siam.
 Milano, F., Dörfler, F., Hug, G., Hill, D.J., and Verbič, G. (2018). Foundations and challenges of low-inertia systems. In *2018 Power Systems Computation Conference (PSCC)*, 1–25. IEEE.
 Poolla, B.K., Bolognani, S., and Dörfler, F. (2017). Optimal placement of virtual inertia in power grids. *IEEE Transactions on Automatic Control*, 62(12), 6209–6220.
 Poolla, B.K., Gross, D., and Dörfler, F. (2019). Placement and implementation of grid-forming and grid-following virtual inertia and fast frequency response. *IEEE Transactions on Power Systems*.
 Rolim, J.G. and Machado, L.J.B. (1999). A study of the use of corrective switching in transmission systems. *IEEE Transactions on Power Systems*, 14(1), 336–341.
 Sadat, S.A. and Sahraei-Ardakani, M. (2018). Reducing the risk of cascading failures via transmission switching. *arXiv preprint arXiv:1810.00651*.
 Shao, W. and Vittal, V. (2005). Corrective switching algorithm for relieving overloads and voltage violations. *IEEE Transactions on Power Systems*, 20(4), 1877–1885.
 Song, Y., Hill, D.J., and Liu, T. (2017). Network-based analysis of small-disturbance angle stability of power systems. *IEEE Transactions on Control of Network Systems*.
 Ulbig, A., Borsche, T.S., and Andersson, G. (2015). Analyzing rotational inertia, grid topology and their role for power system stability. *IFAC-PapersOnLine*, 48(30), 541–547.
 Zhou, K., Doyle, J.C., Glover, K., et al. (1996). *Robust and optimal control*, volume 40. Prentice hall New Jersey.
 Zhu, L. and Hill, D.J. (2018). Stability analysis of power systems: A network synchronization perspective. *Siam Journal on Control & Optimization*, 56(3), 1640–1664.